Journal of the European Ceramic Society 16 (1996) 287–292

0955-2219(95)00153-0
0955-2219/96/$15.00

High Temperature Behaviour of Polycrystalline Aluminosilicate Fibres with Mullite Bulk Composition. II. Kinetics of Mullite Formation

B. O. Hildmann, H. Schneider & M. Schmücker

German Aerospace Research Establishment (DLR), Institute for Materials Research, D-51140 Köln, Germany

(Accepted 22 July 1995)

Abstract

Kinetics and mechanisms of mullite formation in technical diphasic aluminosilicate fibres (Nextel™ 440), consisting of transition alumina and a non-crystalline silica-rich phase, were studied by quantitative X-ray phase analysis. The as-received fibres were heat-treated in the temperature and time ranges from 1130 to 1215°C and from 7·5 min to 32 h. The overall mullitization process can be described by an Avrami reaction law, or alternatively, by a simple exponential reaction law with a temperature-dependent induction period. Early stages of mullite formation with a low mullitization degree ($\alpha = 0{\cdot}02$) are characterized by an activation energy of ~650 kJ mol^{-1}, whereas the apparent activation energy of the overall transformation reaction is ~900 kJ mol^{-1}. Both activation energies are significantly lower than those described in the literature for other diphasic aluminosilicate gels. The relatively low activation energies of mullite formation in Nextel 440 fibres are attributed to the small B_2O_3 content of the as-received fibres. The presence of B_2O_3 may be responsible for the decrease of viscosity of the coexisting non-crystalline SiO_2-rich phase, by which diffusion, and mullite nucleation and growth is accelerated.

1 Introduction

Nextel™ 440 aluminosilicate fibres in the as-received state are diphasic and consist of nanocrystalline transition alumina (γ-Al_2O_3) and a non-crystalline silica-rich phase, which contains 2 wt% B_2O_3. Above 1100°C these fibres transform into mullite which is associated with a distinct drop of tensile strength from about 2·0 to 1·6 GPa. A detailed description of the temperature-dependent microstructural development and related mechanical properties is presented in Part I of this study.[1]

Mullite formation processes from diphasic gels in the system Al_2O_3–SiO_2 have been investigated by several groups (e.g. Refs 1–7). Wei and Halloran[4] studied reaction kinetics and phase transformation mechanisms of a diphasic gel by quantitative X-ray diffraction of annealed samples and described the kinetics by an Avrami equation with an average time exponent $<n>$ = 1·3(2) and a temperature-dependent induction period. Li and Thomson[5] analysed the kinetic mechanisms from different sol–gel precursors using dynamic X-ray diffraction and differential thermal analysis (DTA) methods and found a significant change in the Avrami exponent n. Huling and Messing[6] investigated 'hybrid' gels and analysed the influence of various seedings on the crystallization of aluminosilicate phases. However, no information is available so far on phase transformations in technical Nextel 440 fibres containing some B_2O_3. Information on transformation kinetics and mechanisms is valuable for evaluation of the temperature application range of the fibres, and may also help to understand the microstructural developments of the fibres.

2 Experimental

2.1 Sample material

Continuous Nextel 440 fibre bundles (3M Inc., St. Paul, MN, USA) were used for this study. The chemical composition of the fibres is 70 wt% Al_2O_3, 28 wt% SiO_2 and 2 wt% B_2O_3.[8] The as-received fibres have elliptical cross-sections (mean diameters are 7 and 12 μm), and consist of transition alumina (designated as 'γ-Al_2O_3' in the following) and a coexisting silica-rich, non-crystalline phase.

2.2 Annealing experiments

Annealing experiments were performed in an induction heated laboratory furnace with SiC

susceptor tube at 1128, 1148, 1166, 1183, 1192 and 1215°C under normal air atmosphere conditions. The annealing times ranged between 7·5 min and 32 h with about six different time intervals for each temperature. Furnace temperatures were controlled using a conventional PID controller and a $Pt_{100}/Pt_{90}Rh_{10}$ thermocouple located close to the sample. By means of an additional reference thermocouple, the accuracy of measurements was estimated to be better than ± 3°C. For the annealing experiments a sample of ~1 g fibre was loaded in a small Al_2O_3 crucible and placed into the hot induction furnace. Special care was taken to bring the samples immediately to the annealing temperatures and to quench to room conditions at the end of annealing time.

2.3 X-ray diffraction (XRD)

XRD studies were performed with a computer-controlled Siemens D 5000 diffractometer, equipped with a graphite monochromator in front of the counter. Diffraction patterns were recorded at room temperature with CuK_α radiation in the 2θ range between 25 and 71°. To reduce scattered background intensity, flat silicon single crystal sample holders were used, orientated in such a way that no Si reflection appeared over the 2θ scan region. Following standard procedures in quantitative X-ray analysis[9,10] for determining weight fractions of transformed mullite, calibration XRD reference measurements were recorded from defined mixtures of as-received fibres (not transformed) and fibres that had been heat-treated at 1230°C (completely transformed into the mullite phase). Calibration curves were obtained from integrated intensities of the mullite reflection doublets 120/210, 121/211, 230/320 and from the integrated diffraction intensity of the 400 reflection of transition alumina (γ-Al_2O_3). Based on these calibration curves, the degree of transformation could be determined with an estimated error of ± 1%.

3 Results and Discussion

According to X-ray diffraction spectra and transmission electron microscopic observations, the as-received fibres consist of transition alumina (γ-Al_2O_3) and a non-crystalline SiO_2-rich phase, containing 2 wt% B_2O_3. The phase assemblage directly transforms to mullite in a temperature interval extending from ~1100 to ~1230°C without forming any other transient crystalline phase. The experimentally determined transformation levels α (α = weight fraction of newly formed mullite) are plotted vs. annealing time at different annealing temperatures in Fig. 1 in a semi-logarithmic scale. The fitted curves represent both simple exponential and sigmoidal functions and will be discussed in Section 3.2.

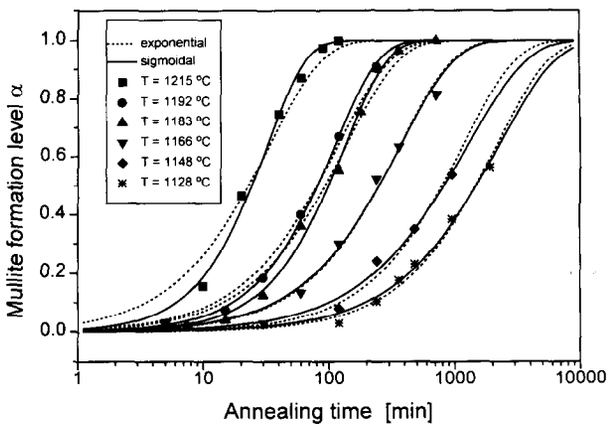

Fig. 1. Experimentally determined mullite formation levels α (weight fraction) plotted as function of annealing time on a logarithmic time scale. Dotted and solid lines correspond to exponential and sigmoidal approximations, respectively, assuming no induction periods ($\tau = 0$) (see Section 3.2).

3.1 Early stages of reaction

Independent from any particular kinetic law, early reaction stages of mullite formation were evaluated by analysing time intervals τ required to attain small, but definite transformation levels α. Though being of major interest, precise determination of formation time intervals τ for very small conversion levels ($\alpha < 0{\cdot}02$) turned out to be difficult, due to the lack of precisely measured data at the very beginning of the transformation processes. Therefore reaction time intervals necessary for the formation of 2, 5 and 10 wt% mullite (α = 0·02, 0·05 and 0·10) were determined from isothermal data sets by interpolating between zero and the first measured data points using linear, polynomial and sigmoidal interpolation functions. Transformation time intervals $\tau_{\alpha = 0{\cdot}02}(T)$, $\tau_{\alpha = 0{\cdot}05}(T)$ and $\tau_{\alpha = 0{\cdot}10}(T)$ belonging to mullite formation levels α = 0·02, 0·05 and 0·10, respectively, are plotted in an Arrhenius diagram in Fig. 2. From the slopes of the fitted straight lines slightly increasing activation energies are obtained with the increase of the transformation level: $\Delta E(\tau_{\alpha = 0{\cdot}02})$ = 644(18) kJ mol^{-1}, $\Delta E(\tau_{\alpha = 0{\cdot}05})$ = 679(12) kJ mol^{-1}, and ΔE $(\tau_{\alpha = 0{\cdot}10})$ = 696(17) kJ mol^{-1}.

Formation time intervals $\tau_{\alpha = 0{\cdot}02}(T)$ certainly cover the early (induction) stages of the transformation processes, including the period of stable nuclei formation and beginning of grain growth. The activation energy of initial mullite formation in Nextel 440 fibres at transformation level α = 0·02 [$\Delta E(\tau_{\alpha = 0{\cdot}02})$ = 644(18) kJ mol^{-1}] is significantly lower than the corresponding value

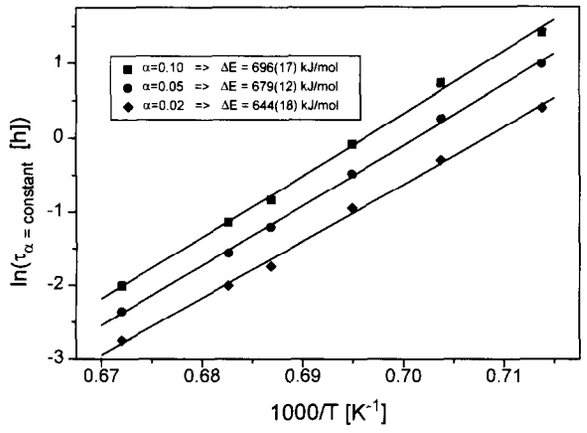

Fig. 2. Arrhenius plot of mullite formation times $\tau_{\alpha = 0.02}(T)$, $\tau_{\alpha = 0.05}(T)$ and $\tau_{\alpha = 0.10}(T)$ required to attain mullite formation levels α = 0·02, 0·05 and 0·10, respectively. An activation energy of ~ 650 kJ mol^{-1} is determined for the early mullite formation stages.

obtained under the same conditions by Wei and Halloran [$\Delta E(\tau_{\alpha = 0.02})$ = 987(15) kJ mol^{-1}][4] for the transformation of diphasic aluminosilicate gels to mullite. The large difference of almost 350 kJ mol^{-1} between both ΔE values can be explained by different nucleation characteristics: a very high nucleation density of about 2 × 10^{15} cm^{-3} is observed in Nextel 440 fibres,[1] which is four orders of magnitude higher than that in diphasic gels, ~ 2 × 10^{11} cm^{-3}.[4] The high nucleation density in the Nextel 440 fibres may be caused by the occurrence of a non-crystalline silicate phase of low viscosity in the transformation interval due to the presence of ~ 2 wt% B_2O_3. Thereby diffusion processes are accelerated by liquid phase assisted mechanisms.

Aksay[11] investigated the diffusion of Si and Al in mullite (and other aluminosilicates) and found that the activation energy for the diffusion of Si and Al species alone amounts to ~700 kJ mol^{-1} which is sightly higher than our experimentally obtained value for the initial processes in Nextel 440 fibres. A conclusion is either that in our case (1) the additional activation energy term for nuclei formation is negligibly small, or (2) diffusion barriers play a less important role than they do usually in the initial stages of mullite formation, due to the presence of B_2O_3.

3.2 Overall transformation laws

In the discussion of the kinetics of the overall mullite formation processes, we used rate equations of the general form:[12]

$$K(T)\cdot(t - \tau) = f(\alpha) \qquad (1)$$

with α = transformation level (weight fraction of newly formed mullite), K = reaction rate parameter, t = annealing time and τ = induction period.

In a first approach the kinetic data were fitted using a simple exponential function (index e). Such transformation laws are characteristic for chemical first-order reactions and have often been used to describe diffusion controlled grain growth processes:

$$K_e(T)\cdot(t - \tau) = -\ln(1 - \alpha) \qquad (2)$$

The dashed curves in Fig. 1 are least-squares fits using Eqn (2), but without considering any induction period (τ = 0). In a ln(1 − α) vs. t diagram, not shown here, linear regression lines are obtained documenting a reasonable fit of measured and calculated data. Refined values for K_e are summarized in Table 1.

A closer look at the kinetic data shows that the transformation curves do not really follow the simple kinetic law of Eqn (2) with τ = 0, but display sigmoidal shapes (index s). Transformation curves of this type are described by a modified Avrami kinetic law:[12]

$$K_s(T)\cdot(t - \tau) = [-\ln(1 - \alpha)]^{1/n} \qquad (3)$$

Compared with Eqn (2), Eqn (3) has a time exponent n (real number) as an additional freely

Table 1. Kinetic data evaluation of the overall mullite formation: reaction rate coefficients K and exponents n for one exponential and two sigmoidal approximations of the kinetic Avrami law in the general form $K\cdot(t - \tau) = [-\ln(1 - \alpha)]^{1/n}$. In one sigmoidal approximation induction periods $\tau = \tau_{\alpha = 0.02}$ were assumed. The numbers in parenthesis represent standard deviations from least-squares refinements and refer to the last digits.

Annealing temperature, T (°C)	*Exponential approximation* (n = *1*): $ln(1 - \alpha) = -K_e\cdot t$		*Sigmoidal approximations* (n ≠ *1*): $ln[-ln(1 - \alpha)] = n\cdot ln(K_s) + n\cdot ln(t - \tau)$				
	No induction period, τ = *0*		*No induction period*, τ = *0*		*Induction period*, $\tau = \tau\alpha$ = *0·02*		
	K_e	$ln(K_e)$	$n\cdot ln(K_s)$	n	$n_\tau\cdot ln(K_{s\tau})$	n_τ	$\tau_{\alpha = 0.02}$ (h)
1215	2·27(10)	0·82	0·87(18)	1·59(13)	0·869(52)	1·11(3)	0·064
1192	0·585(15)	−0·54	−0·83(10)	1·373(84)	−0·502(36)	0·98(3)	0·135
1183	0·539(21)	−0·62	−1·113(63)	1·367(63)	−0·671(56)	1·03(4)	0·175
1166	0·1498(64)	−1·90	−2·20(19)	1·23(13)	−1·511(36)	0·88(2)	0·39
1148	0·0504(23)	−2·99	−3·00(31)	1·03(16)	−2·46(12)	0·82(7)	0·75
1128	0·02727(95)	−3·60	−3·94(27)	1·15(12)	−2·907(31)	0·81(2)	1·5
mean of *n*				1·29(20)		0·94(12)	

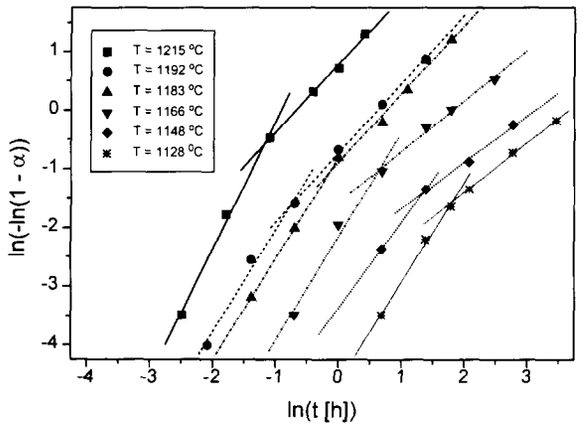

Fig. 3. Mullite formation levels α plotted in the form ln[–ln (1 – α)] vs. ln(t) without considering any induction period [τ = 0]. It is obvious that the measured data is not well fitted by one straight line, but 'initial' and 'final' regions can be distinguished.

refined parameter, and an induction period τ. The solid lines in Fig. 1 are least-squares fits using Eqn (3), again without considering any induction period (τ = 0). Compared with the exponential approach the sigmoidal functions represent better numerical approximations. Refined values for n [average $<n>$ = 1·3(2)] and $n \cdot K_s(T)$ are listed in Table 1.

If the measured raw data are plotted in double logarithmic plots, ln[–ln(1 – α)] vs. ln(t), it becomes obvious that one single straight line for each isothermal data set does not fit the data well (see Fig. 3). Instead, two straight lines with significantly different slopes n referring to an 'initial' (index 1) and a 'final' (index 2) transformation region* can be distinguished ('split model'). Linear regression fits for the two transformation regions lead to values $n_1 \cdot \ln(K_1)$ and n_1 [average $<n_1>$ = 1·81(18)] and to $n_2 \cdot \ln(K_2)$ and n_2 [average $<n_2>$ = 1·00(20)], respectively.

Several possible explanations for the change of slopes n were discussed in the literature. Arguments are based on the ideas that (1) nucleation sites are consumed in the 'initial' region,[13] (2) variable nucleation and growth rates occur in different grains,[14] and (3) impingement of growing grains takes place in the 'final' region.[15] Li and Thomson described a significant change in the Avrami slope for a diphasic gel[5] (from $<n_1>$ = 2 to $<n_2>$ = 0·5) and a somewhat smaller change for a single-phase gel[16] (from $<n_1>$ = 1 to $<n_2>$ < 0·4). Li and Thomson[5] explained the change of n in the diphasic gel by impingement of grains in the 'final' region using the model of Rosen *et al.*,[15] who analysed the recrystallization of pure iron and suggested preferred impingement of grains in the axial direction causing the grains to grow only in the transverse direction. Impingement of grains effectively leads to a reduction of growth dimensionality, and thus of slope n, due to restrictions in normal growth directions. Huling and Messing[6] also attributed lower n values to effectively lower dimensional growth, e.g. due to combinations of growth along and normal to the interfaces in diphasic 'hybrid' $75M_I$ gels. In Nextel 440 fibres reduction of growth dimensionality may also take place due to impingement of grains and, thus, explain the change of n. Here, however, the difference of n values between 'initial' and 'final' region [$<n_1>$ = 1·81(18) and $<n_2>$ = 1·00(20)] is smaller than the values reported in the literature.

Another way to treat the change of slopes n is based on the consideration of induction periods $\tau(T)$, which have not been taken into account in our data analyses up to this point and have also not been considered by Li and Thomson.[5,16] In order to check for linearity in ln[–ln(1 – α)] vs. ln(t) plots, induction periods $\tau(T)$ were introduced prior to numerical data evaluation. It should be kept in mind that precise estimations of $\tau(T)$ values are required, and that slight variations of τ sensitively influence the shape of the reaction curves. Such a precise determination of τ from the measured raw data at early reaction stages is difficult (see also Section 3.1). Following the procedure of Wei and Halloran,[4] formation time periods $\tau_{\alpha=0.02}(T)$, required to attain a mullite formation level α = 0·02, were arbitrarily considered as induction periods τ to correct the time axis of the measured isothermal raw data before subsequent calculations. Starting from this point, data sets of $\alpha(T)$ were numerically approximated via least-squares techniques using Eqn (3) in the form

$$\ln[-\ln(1-\alpha)] = n(T) \cdot \ln[K_s(T)] + n(T) \cdot \ln[t - \tau_{\alpha=0.02}(T)] \quad (4)$$

Induction time periods $\tau_{\alpha=0.02}(T)$ and freely refined parameters $n_\tau \cdot K_{s\tau}$ and n_τ are listed in Table 1. Mullite formation levels α presented in double logarithmic plots now yield straight lines. The lines have slightly different slopes $n_\tau(T)$ ranging around a mean value of $<n_\tau>$ = 0·94(12) (see Fig. 4). Since n_τ is close to 1 in each case mullite formation can be equally well described by a first-order reaction (n = 1), if correct temperature-dependent induction periods $\tau_0(T)$ are taken into account. Finally, refinements with fixed n = 1 and slightly changed induction periods $\tau_0(T)$ confirm this conclusion. We believe that this simple kinetic model is best suited to describe the mullite formation processes in Nextel 440 fibres.

Arrhenius plots fitted on the basis of least-squares regressions of experimentally determined

*The 'initial region' extends up to a transformation level of 20 to 35 wt%. It should not be mixed up with the term 'induction period', which characterizes the early beginning of the reaction (α < 0·02).

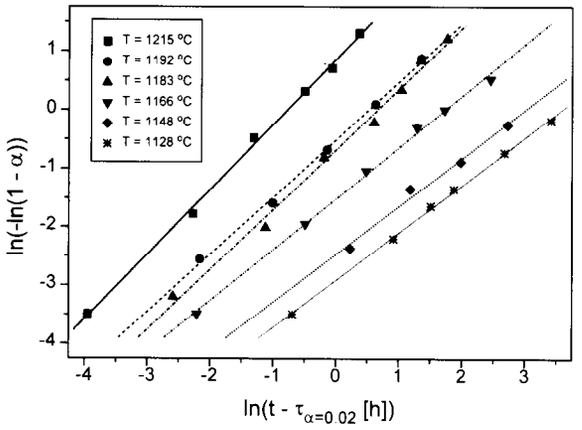

Fig. 4. Mullite formation levels α plotted in the form $\ln[-\ln(1-\alpha)]$ vs. $\ln(t-\tau)$. Induction times $\tau = \tau_{\alpha=0.02}(T)$ were used to correct the time axis prior to numerical fitting. Linear regression fits yield values $n_\tau \cdot \ln(K_{s\tau})$ and n_τ listed in Table 1 (compare with Fig. 3).

rate coefficients $\ln(K_e)$ and $\ln(K_{s\tau})$ are shown in Fig. 5 (see Table 1). From the slopes of the straight lines apparent activation energies of the overall mullite formation processes can be derived. Based on reaction rate coefficients K_e and $K_{s\tau}$, the values ΔE_e = 914(56) kJ mol^{-1} and $\Delta E_{s\tau}$ = 903(54) kJ mol^{-1} are obtained, respectively. An Arrhenius plot of $n \cdot \ln(K_s)$ leads to the energy value 939(56) kJ mol^{-1}. From Arrhenius plots of $\ln(K_1)$ and $\ln(K_2)$ of the 'split model', apparent activation energies ΔE_1 = 727(59) kJ mol^{-1} and ΔE_2 = 908(64) kJ mol^{-1} were calculated. Compared with the activation energy of the inital stages of reaction (derived from Arrhenius plots of formation times $\tau_{\alpha=0.02}$, see Section 3.1), the apparent activation energies for the overall mullite forming processes [derived from Arrhenius plots of the reaction coefficients $\ln(K)$] are clearly higher. This indicates that processes associated with initial nucleation and grain growth are characterized by smaller energy barriers than those related to final formation and grain growth.

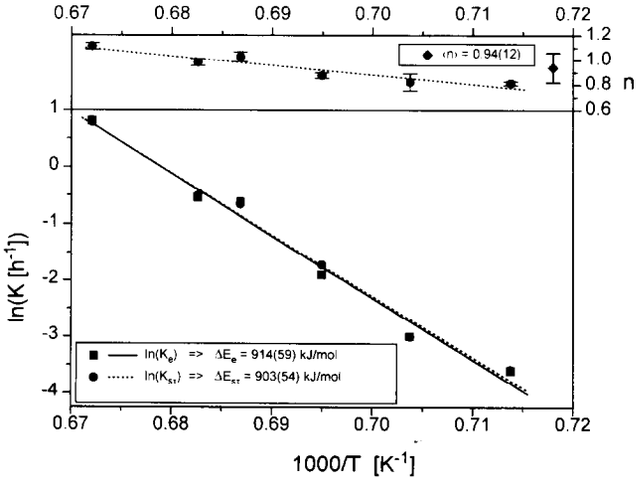

Fig. 5. Arrhenius plot of $\ln(K_e)$ (exponential approximation) and $\ln(K_{s\tau})$ (sigmoidal approximation considering induction periods $\tau = \tau_{\alpha=0.02}$) for the overall mullite transformation. The different slopes give apparent activation energies of ΔE_e = 914(56) kJ mol^{-1} and $\Delta E_{s\tau}$ = 903(54) kJ mol^{-1}. The average value of the exponent n is 0·94(12).

The mean values of the apparent mullite activation energies of Nextel 440 fibres are lower than the mean values of diphasic gels reported in the literature (e.g. Wei and Halloran:[4] ΔE = 1070(200) kJ mol^{-1}; Li and Thomson:[5] ΔE = 1028(37) kJ mol^{-1}; and Huling and Messing:[6] ΔE = 987(71) kJ mol^{-1} for the hybrid gel 25M$_I$). It must be emphasized that Wei and Halloran obtained their value from an Arrhenius plot of $n_\tau \cdot \ln(K_{s\tau})$ considering induction periods $\tau = \tau_{\alpha=0.02}$ before data evaluation, whereas Huling and Messing obtained theirs from an Arrhenius plot of $\ln(K_s)$ without considering an induction period. Li and Thomson obtained their value from DTA measurements. The differences between apparent activation energies of mullitization between the present study and literature data may have similar reasons as already discussed for the initial stages of reaction (see Section 3.1). A suitable explanation is that atomic diffusion, which is the rate-controlling process for both nucleation and growth, is enhanced in Nextel 440 fibres by the presence of the viscous glassy phase containing B_2O_3, which, according to our observations, is retained in the bulk of the fibres at least up to 1400°C. Our own preliminary studies have also shown that diphasic fibres without B_2O_3 (Nextel^{TM} 550, Altex from Sumitomo Chemical Inc.) transform into mullite in a similar way as do, for example, Wei and Halloran's diphasic (but B_2O_3-free) gels, thus supporting the suggestion that B_2O_3 content has a transformation-controlling influence.

References

1. Schmücker, M., Flucht, F. & Schneider, H., High temperature behaviour of polycrystalline aluminosilicate fibres with mullite bulk composition, I. Microstructure and strength properties. *J. Eur. Ceram. Soc.*, **16** (1996) 281–5.
2. Hoffmann, D. W., Roy, R. & Komarneni, S., Diphasic xerogels, a new class of materials in the system Al_2O_3–SiO_2. *J. Am. Ceram. Soc.*, **67** (1984) 468–71.
3. Wei, W. & Halloran, J. W., Phase transformation of diphasic aluminosilicate gels. *J. Am. Ceram. Soc.*, **71** (1988) 166–72.
4. Wei, W. & Halloran, J. W., Transformation kinetics of diphasic aluminosilicate gels. *J. Am. Ceram. Soc.*, **71** (1988) 581–7.
5. Li, D.X. & Thomson, W. J., Kinetic mechanisms for mullite formation from sol–gel precursors. *J. Mater. Res.*, **5** (1990) 1963–9.
6. Huling, J. C. & Messing, G. L., Epitactic nucleation of spinel in aluminosilicate gels and its effect on mullite crystallization. *J. Am. Ceram. Soc.*, **74** (1991) 2374–81.
7. Voll, D., Mullitprecursoren: Synsthese, temperaturabhängige Entwicklung der strukturellen Ordnung und Kristallisationsverhalten. PhD thesis, University of Hannover, 1994.

8. 3M Company, *Properties of Nextel™ 440 ceramic fibers*. Technical data, 3M Ceramic Materials Department, 1993.
9. Klug, H. P. & Alexander, L. E., *X-ray Diffraction Procedures*. John Wiley, New York, 1954.
10. Cullity, B. D., *Elements of X-ray Diffraction*. Addison-Wesley, London, 1956.
11. Aksay, I. A., Diffusion and phase relationship studies in the alumina silica system. PhD Thesis, University of California, Berkeley, CA, 1973.
12. Bamford, C. H. & Tipper, C. F. H., *Chemical Kinetics–Reactions in the Solid State*. Elsevier Scientific, Amsterdam, 1980, Vol. 22.
13. Avrami, M., Kinetics of Phase Changes II. Transformation–time relations for random distribution of nuclei. *J. Chem. Phys.*, **8** (1940) 212–24.
14. Rollet, A. D., Srolovitz, D. J., Doherty, R. D. & Anderson, M. P., Computer simulation of recrystallization in non-uniformly deformed metals. *Acta Metall.*, **37** (1989) 627–39.
15. Rosen, A., Burton, M. S. & Smith, G. V., Recrystallization of high-purity iron. *Trans. AIME*, **230** (1964) 205–15.
16. Li, D. X. & Thomson, W. J., Mullite formation kinetics of a single-phase gel. *J. Am. Ceram. Soc.*, **73** (1990) 964–9.